Morphometry of SARS-CoV and SARS-CoV-2 particles in ultrathin plastic sections of infected Vero cell cultures

Michael Laue[1*], Anne Kauter[1], Tobias Hoffmann[1], Janine Michel[2], Andreas Nitsche[2]

[1] Advanced Light and Electron Microscopy, Centre for Biological Threats and Special Pathogens 4 (ZBS 4), Robert Koch Institute, Germany

[2] Highly Pathogenic Viruses, Centre for Biological Threats and Special Pathogens 1 (ZBS 1), Robert Koch Institute, Germany

*corresponding author:

Dr. Michael Laue

Advanced Light and Electron Microscopy

Centre for Biological Threats and Special Pathogens 4 (ZBS 4)

Robert Koch Institute

Seestr. 10

D-13353 Berlin

Germany

e-mail: lauem@rki.de

Abstract

SARS-CoV-2 is the causative of the COVID-19 disease, which has spread pandemically around the globe within a few months. It is therefore necessary to collect fundamental information about the disease, its epidemiology and treatment, as well as about the virus itself. While the virus has been identified rapidly, detailed ultrastructural analysis of virus cell biology and architecture is still in its infancy. We therefore studied the virus morphology and morphometry of SARS-CoV-2 in comparison to SARS-CoV as it appears in Vero cell cultures by using conventional thin section electron microscopy and electron tomography. Both virus isolates, SARS-CoV Frankfurt 1 and SARS-CoV-2 Italy-INMI1, were virtually identical at the ultrastructural level and revealed a very similar particle size distribution (~100 nm, without peplomers). SARS-CoV showed a slightly broader size distribution with a few smaller and bigger particles than SARS-CoV-2. The segmental peplomer density of SARS-CoV was approximately 30% higher than the corresponding peplomer density of SARS-CoV-2. This result complements a previous qualitative finding, which was related to a lower productivity of SARS-CoV-2 in cell culture in comparison to SARS-CoV.

Introduction

The Severe Acute Respiratory Syndrome Coronavirus 2 (SARS-CoV-2) is a beta-Coronavirus which entered the human population most probably at the end of 2019 and is spreading pandemically around the world[1]. The virus causes the disease termed COVID-19 which primarily affects the respiratory system[1,2] but can extend to other organs[3]. Severity of the disease is highly variable from non-symptomatic to fatal outcomes[1].

SARS-CoV-2 is genetically similar to SARS-CoV (79% sequence identity[4]) which appeared in the human population in 2003. Both viruses use the same receptor (i.e. the angiotensin-converting enzyme 2, ACE2) for host cell entry[5]. Infection of different cell lines and of patient material could be shown[6,7,8]. Ultrastructural hallmarks of entry, replication and assembly seem to be virtually identical to SARS-CoV[9]. Like all viruses of the family Coronaviridae, the virus is a biomembrane-enveloped virus with prominent spike proteins (S protein), called peplomers, which are arising from the membrane (Fig. 1). The structural biology of the trimeric S protein was already resolved by cryo-electron microscopy (EM)[10]. The virus genome is a single plus-strand RNA molecule which is associated with the nucleoprotein (N protein) in the enveloped lumen of the virus (Fig. 1).

Very recently, morphometric data on isolated SARS-CoV-2 particles[10-13] and virus particles in cells[14], obtained by cryo-EM, were published or became available as a preprint. While cryo-EM is definitely the best method to study virus ultrastructure and structural biology, conventional EM, using plastic embedding, still is of relevance, especially for the study of samples, which cannot be easily analyzed by cryo-EM, such as complex multicellular objects or pathological material obtained from patients. Search of viruses in such material is difficult and needs a suitable reference obtained with virus infected cell culture material using the same preparation technique[15]. To provide reference data for this purpose, we carried out a study on the morphometry of virus particles of SARS-CoV-2 in comparison to virus particles of SARS-CoV by using transmission EM of the virus in thin sections of plastic embedded infected cell cultures.

We show the particle size distribution of virus particle profiles in conventional ultrathin sections and in single-axis tomograms of thicker sections. The peplomer density was determined for virus profiles in very thin ultrathin sections (= small projection volume) to increase visibility of peplomers. The study provides robust data, including all raw data files, on the morphometry of the two coronaviruses as they appear in conventional thin section EM of virus producing cell cultures

and demonstrate that the investigated SARS-CoV and SARS-CoV-2 isolates are very similar in their ultrastructure apart from a small difference in peplomer density.

Methods

Virus isolates

The following virus isolates were used:

(1) SARS Coronavirus Frankfurt 1 (SARS-CoV)[16]

(2) SARS Coronavirus 2 Italy-INMI1 (SARS-CoV-2)[17]

Cell culture

Vero E6 cells (African green monkey kidney epithelial cell, ECACC, ID: 85020206) were cultivated in cell culture flasks with D-MEM, including 1% L-glutamine and 10% fetal bovine serum, for 1 d at 37 °C and 5% CO_2 to reach approximately 70% confluence. To infect the cultures with virus, the medium was removed and 10 ml of fresh medium with diluted virus stock suspension was added to the cells. After incubation for 30 min, as indicated above, 20 ml of medium was added and cells were further incubated. Cultivation was stopped 24 h after addition of the virus suspension by replacing the medium with 2.5% glutaraldehyde in 0.05 M Hepes buffer (pH 7.2). Incubation with the fixative lasted at least 1 h at room temperature. Fixed cells were scraped from the culture flasks and collected in centrifuge tubes.

Electron microscopy (EM)

Fixed cells were sedimented by centrifugation (3000 g, 10 min) using a swing-out rotor and washed twice with 0.05 M Hepes buffer. The cell pellet was heated to 40 °C in a water bath and mixed with 3% low-melting point agarose (1:1 [v/v]) at 40 °C. After a brief (approx. 2-3 min) incubation at 40 °C, the suspension was centrifuged in a desktop centrifuge using a fixed-angle rotor for 5 min at 5000 g and cooled on ice to form a gel. The cell pellet was cut off from the agarose gel block by using a razor blade and stored in 2.5% glutaraldehyde in 0.05 M Hepes buffer. Postfixation, block contrasting, dehydration and embedding in epoxy resin (Epon[18]) were done following a standard protocol[19] (Supplementary Table 1).

Ultrathin sections were produced with an ultramicrotome (UC7, Leica Microsystems, Germany) using a diamond knife (45°, Diatome, Switzerland). Sections were collected on bare copper grids (300 mesh, hexagonal mesh form), contrasted with 2% uranyl acetate and 0.1% lead citrate and coated with a thin (2-3 nm) layer of carbon. For electron tomography, gold colloid (15 nm cationic

gold; 1:10 to 1:20) was added to the carbon-side of the sections by incubating the sections on a drop of the gold colloid suspension for 1-5 min at room temperature.

EM of thin sections was performed with a transmission electron microscope (Tecnai Spirit, Thermo Fisher Scientific) which was equipped with a LaB_6 filament and operated at 120 kV. Magnification calibration of the microscope was done by using the MAG*I*CAL calibration reference standard for TEM (Technoorg Linda, Hungary). Images were recorded with a side-mounted CCD camera (Megaview III, EMSIS, Germany) at a resolution of 1376 x 1032 pixel. Tilt series for electron tomography were acquired by using the tomography acquisition software of the Tecnai (Xplore 3D v2.4.2, Thermo Fisher Scientific) and a bottom-mounted CCD camera (Eagle 4k, Thermo Fisher Scientific) at a resolution of 2048 x 2048 pixel. A continuous tilt scheme at one degree interval was used and at least 120 images were recorded (minimum +60 to -60°). Tracking before image acquisition was performed to compensate image shifts introduced by the mechanics of the stage. Alignment and reconstruction were done with the Inspect3D software (Version 3.0; Thermo Fisher Scientific) by using a defined procedure and the “Simultaneous Iterative Reconstruction Technique“ (SIRT) with 25 iterations (Supplementary Table 2).

Measurement of virus particle size

Size of virus particle profiles was measured in images of ultrathin (60-70 nm) sections and in tomograms of thin (150-180 nm) plastic sections.

Extracellular virus particles in ultrathin sections were selected randomly at the microscope and were recorded with the side-mounted camera (at a magnification of 105,000x), if they met the following criteria: (1) the particle was morphologically intact; (2) the particle was not pressed against other structures; (3) at least 2/3 of the virus particle was covered with peplomers. Three datasets were recorded (see Table 1).

Size measurements were done with the iTEM software (version 5.2; EMSIS, Germany) and the “Circle with Center and Radius“ measurement function (mouse adjustable radius). The circle radius was adjusted to fully enclose the particle (with and without peplomers) and the radius was determined, which corresponded to the maximal diameter of the virus particle profile. Extracellular virus particles in thin sections were recorded by single-tilt electron tomography using the bottom-mounted Eagle 4k CCD camera, at a magnification of 18,500x and 23,000x (1.17 and

0.96 nm pixel size) and a binning of 2. Virus particles were selected randomly. If particles appeared morphologically intact and tilting to at least -60 and +60° was possible, a tilt series of the region of interest was recorded. Two datasets, one for SARS-CoV and one for SARS-CoV-2, with a minimum of 12 tilt series each, were recorded (Table 1). Tomograms were reconstructed according to the workflow listed in Supplemental Table 2. Measurements were performed with the Fiji software[20] by using the following workflow. Tomograms were loaded, size calibrated and inspected in the orthoslice view (z, x/z and y/z view). For size measurements, particles were selected which appeared intact, showed no distinct compression by other structures and which were with more than half of their size enclosed in the tomogram volume. Maximal diameter of the selected virus particle (without peplomers) was measured by adjusting the z view to a level where the particle in x/z and y/z view becomes maximal in width and by using the oval selection tool with the measurement setting „fit ellipse“. The maximal diameter of the oval (elliptical) selection was noted.

Measurement of peplomer density

The peplomer density on virus particles was estimated using very thin (45 nm) plastic sections. Extracellular virus particles were randomly selected and recorded with the side-mounted CCD camera at a magnification of 135.000x if the particles met the following criteria: (1) the particle was morphologically intact; (2) the particle was not deformed (e.g. by pressing against other structures); (3) the particle membrane was visible (at least 90% of the perimeter). Two datasets, each with about 150 particles, were recorded (see Table 1).

To determine the number of peplomers per membrane profile length, the perimeter of each virus particle was manually outlined with the “Fitted Polygon“ measurement function of the iTEM software (version 5.2; EMSIS, Germany) and measured, while the peplomers (including partially visible peplomers) were counted. Number of peplomers per membrane profile length was normalized to a membrane length of 320 nm which was approximately the median perimeter length of the virus particle profile in very thin plastic sections. The resulting values represent the peplomer density per unit perimeter length and the segmental particle volume present in the section and is termed “segmental peplomer density“ of virus particles.

Table 1. Overview of the datasets used for virus particle measurements

Dataset #	Virus isolate	Sample	Number of sections	Section thick-ness [nm]	Number of files	File format	Pixel size [nm]
1	SARS-CoV Frankfurt	A	4	60-70	126	tif, 16 bit	0.64
2	SARS-CoV-2 Italy-INMI1	B	4	60-70	128	tif, 16 bit	0.64
3	SARS-CoV-2 Italy-INMI1	C	5	60-70	122	tif, 16 bit	0.64
4	SARS-CoV Frankfurt	A	2	150-180	12	mrc/tif, 16 bit	0.96 / 1.17
5	SARS-CoV-2 Italy-INMI1	B	3	150-180	17	mrc/tif, 16 bit	0.96 / 1.17
6	SARS-CoV Frankfurt	A	5	45	111	tif, 16 bit	0.54
7	SARS-CoV-2 Italy-INMI1	B	5	45	134	tif, 16 bit	0.54

Results

Extracellular virus particles of SARS-CoV and SARS-CoV-2 in Vero cell cultures revealed no significant morphological differences in ultrathin sections (Fig. 2). Virus particles appear as round to oval profiles. Size distributions of virus particle profiles in conventional ultrathin (60-70 nm) sections were also similar for both viruses (Fig. 3 A-D). SARS-CoV showed a few smaller and larger profiles than SARS-CoV-2, which could be due to the presence of a few particles with a non-circular/-oval shape (see below). However, the median of maximal particle profile was the same (130 nm with peplomers and 90 or 89 nm without peplomers) for both viruses. The replication of the analysis using a second cell culture batch in an independent infection experiment with SARS-CoV-2 resulted in an essentially identical size distribution and median of the particle profiles (Supplemental Fig. S1).

The size distribution, and especially the median, resulted by measuring the virus particle profiles in conventional ultrathin sections could be biased by an overrepresentation of virus section profiles of a particular virus particle size and by deformed particles. Therefore, we recorded tomographic tilt series of viruses in thicker sections (150-180 nm) and calculated single-axis tomograms to measure virus particles at their maximal diameter (Fig. 4) and to rule out the presence of deformed (i.e. non-circular/-oval) virus particles. The aligned tilt series and the tomograms showed that almost all of the particles possessed an oval shape (Supplemental Videos 1-4). We rarely (less than 5% of all particles) detected deformed particles. In the SARS-CoV samples we found one small cluster of deformed viruses attached to a cell (Supplemental Fig. S2) which were excluded from the measurements. Due to the variable and frequently low density of the peplomers, we only measured the maximal particle size without peplomers in the tomograms. Particle size distribution determined in tomograms is similar to the particle size distribution measured in ultrathin sections (Fig. 3 C-F), with again an identical median for SARS-CoV and SARS-CoV-2 of 99 nm, which is approximately 10 nm more than measured in thin sections. The size distribution was also similar with a slight shift to higher particle diameter for the SARS-CoV (Fig. 3E, F). We have to note that the thin sections shrunk during electron beam illumination which caused a compressed appearance of the particles in x/z and y/z direction (Fig. 4). This effect is well known and usually does not affect dimensions in x/y if samples/sections are well fixed at their supports[21], which most likely was the case during our image recording because we used sections on grids with rather small holes and finally stabilized the sections by a carbon layer.

To get an idea about the peplomer density on the two different coronaviruses, we counted the

peplomers present on particle profiles in very thin (45 nm) sections and related the number to the membrane length of the particle perimeter (segmental peplomer density). The measurements were normalized to a reference perimeter membrane length of 320 nm, which corresponds to the median particle profile perimeter measured in the analysis. Figure 5 shows two representative virus particles of the datasets. The frequency distribution of the segmental peplomer density for the two coronaviruses revealed a similar shape with a shifted median, i.e. SARS-CoV = 12 and SARS-CoV-2 = 9 peplomers per reference perimeter membrane length. Although the frequency distributions of the segmental peplomer density were widely overlapping (Fig. 5 C, D), measurements indicated that the investigated SARS-CoV virus population carried more peplomers at their surface than the SARS-CoV-2 virus population.

Discussion

We determined the size and peplomer density of SARS-CoV and SARS-CoV-2 virus particles *in situ,* in the surrounding of virus producing Vero cells, by using thin section EM. Viruses and cells were chemically inactivated and stabilized by glutaraldehyde *in situ* and embedded in plastic. This preparation procedure changes the ultrastructure of biological objects[22], including their dimensions[23], e.g. by adding chemicals or by removing the water, and it does not preserve their accurate molecular structure[24]. However, at the resolution level sufficient to study the ultrastructure of organelles (i.e. their shape and internal architecture), this procedure provides reliable information which is, at this resolution, in many cases very similar to the information obtained by cryo-EM[22], the gold standard in structural biology.

Cryo-EM provides maximal structural information about the virus architecture down to the molecular level[25,26]. However, for single particle cryo-EM, virus particles usually have to be concentrated and purified, which is not trivial, especially for enveloped viruses. Purification and/or enrichment can select for a certain particle size and shape, introduce deformations[27], which was also observed for SARS-CoV-2[11], and might cause loss of membrane protein[28]. Biosafety still requires inactivation of the virus preparation before conducting the sample preparation for cryo-EM, and the effects on the ultrastructure must be carefully controlled. The recently published work on isolated SARS-CoV-2[11-13] only partially addressed those aspects[11].

Studying virus particles by cryo-EM *in situ* attached to or present in the cells is extremely difficult to perform, since whole cell cryo-EM (i.e. cryo-electron tomography) needs either thin parts of an infected cell or lamella preparation by FIB-SEM to generate datasets of frozen hydrated and therefore virtually unchanged virus particles[29]. This work is technically extremely challenging and very time consuming[29] and usually restricted to a limited set of samples which not necessarily fully represent the biological variability of the sample. However, in a recent study both approaches could be applied to SARS-CoV-2 infections of different cell lines[14] providing valuable structural data on cell-associated virus.

Our study was intended to provide a reference for ultrastructural work performed on virus infected cells embedded in plastic, because this method is widely used to study, for instance, the cell biology of infection models or infected patient material. The results revealed that the SARS-CoV and SARS-CoV-2 are very similar in morphology and size, as could be expected from the close

taxonomic relationship of the two viruses[4] and reports on the virus ultrastructure in plastic sections which are available[8,9,15]. However, the similarity of the size distribution of the two coronaviruses tested and of the two biological replicates (two independent infection experiments with SARS-CoV-2) was a surprise because enveloped viruses are usually more variable in shape and size than non-enveloped viruses[30]. We used two different strategies for determination of virus particle size in thin sections: (1) Measurement of virus particle section profiles in ultrathin (60-70 nm) sections and (2) measurement of widest particle profile in tomograms of thin (150-180 nm) sections. The size distribution median was about 10 nm bigger in tomograms than in ultrathin sections, which can be explained by the fact that in ultrathin sections the smaller profiles of a dominant fraction of particles that are larger than the section thickness will be overrepresented in the analysis and shift the size distribution to lower values. The median of the size distribution of virus particles without peplomers in tomograms was about 100 nm for both coronavirus isolates and can be estimated to be about 140 nm with peplomers, based on the measurements of particle section profiles in ultrathin sections which indicate a peplomer size of about 20 nm in our samples.

The size values measured for SARS-CoV in our study (~100 nm, without peplomers) differ from the values measured by cryo-EM (SARS-CoV: 86.5 nm[31] ; SARS-CoV-2: 90-97 nm[11,13,14]). As already mentioned above, it is highly likely that the plastic embedding changed the size of the virus particles. For instance, it is known that the tannic acid and bloc-contrasting scheme which we have used increases membrane thickness[32] and that tannic acid binds to glycoproteins[33] such as the S-protein, which could account for the observed differences in size. Other reasons to explain the difference could be the different virus strains which we have used in comparison to the strains used in the cryo-EM studies[11,13,14,31] or differences in the cell culture. It is also not possible to exclude that concentration and purification of virus particles before cryofixation have an impact on the size distribution of the virus particle population. A comparison of non-purified and purified SARS-CoV-2 showed only small differences (91 vs. 92 nm[11]) and the measurement of SARS-CoV-2 *in situ* resulted in similar values (90 nm[14]) which suggest that virus particles were not affected during preparation in those experiments. In contrast, the cell type producing the virus seems to have an effect on the size distribution[11].

In summary, the particle size of SARS-CoV and SARS-CoV-2 measured by conventional thin section EM is only roughly 10% different from the particle size values obtained by cryo-EM. Even the size of the peplomers is similar with both methods (~20 nm). Remarkably, negative staining EM of entire virus particles of the same SARS-CoV-2 isolate as the one used for determination of particle size in

thin plastic sections, revealed size values (90 nm; Supplemental Methods and Supplemental Fig. S3) which are practically identical to the values measured by cryo-EM (~90 nm[11,14]).

The measurement of the peplomer number in a small volume of sectioned particles, which can be termed "segmental peplomer density", revealed differences which could reflect differences in peplomer density of virus particles of the two different coronavirus populations studied. A qualitative difference of the peplomer density between SARS-CoV and SARS-CoV-2 was already observed in another study[9] and associated with a reduced infectivity of SARS-CoV-2 in comparison to SARS-CoV. Our quantitative measurements, which were performed with the same SARS-CoV isolate but a different SARS-CoV-2 isolate than the one used in the study of Ogando *et al.*[9], support this conclusion. For SARS-CoV, Beniac *et al.*[31] estimated a mean number of 65 peplomers per virus using cryo-EM, with a certain variability in distribution between different particles, which corresponds roughly to the maximum values measured for SARS-CoV in our study. We measured a maximum value of 22 peplomers for a virus segment (45 nm thick), which roughly represents a third of an entire virus particle. However, the median is much lower, i.e. 12 peplomers per virus segment, which indicates differences between the two virus populations analyzed. Again, Beniac *et al.*[31] used a different SARS-CoV isolate than we have used in our study (Tor 3 versus Frankfurt 1), which may explain the observed differences. Peplomer density of SARS-CoV-2 was determined recently by cryo-EM for different virus isolates than the virus isolate used in our study. The reported mean values vary from 25 to 40 peplomers per virus particle with significant variation among particles[11-14]. Our measurements of 9 peplomers per virus segment, representing roughly a third of the entire virus, falls in the same range. The relevance of the difference of the peplomer density between different virus isolates is not known but could be related to virus infectivity and fitness which must be studied further. Our comparatively simple method to achieve a measure for the peplomer density and variability in a virus population could be helpful to analyze the different SARS-CoV-2 isolates already present or evolving in the human population[34] by comparing the peplomer density with virus infectivity and receptor-binding affinities.

In summary, we provide morphometric data for SARS-CoV and SARS-CoV-2 particles in plastic sections, which are very similar to the data obtained by cryo-EM. All raw datasets can be used for re-investigation or other purposes (e.g. for validation / testing / training of computer algorithms). The major outcome is that the investigated isolates of SARS-CoV and SARS-CoV-2 are ultrastructurally very similar in shape and size and show a small difference in their peplomer density.

Data availability

Datasets 01 to 07 (see Table 1) are available at the data repository Zenodo:

Dataset 01: DOI 10.5281/zenodo.3985098

Dataset 02: DOI 10.5281/zenodo.3985103

Dataset 03: DOI 10.5281/zenodo.3985110

Dataset 04: DOI 10.5281/zenodo.3985120

Dataset 05: DOI 10.5281/zenodo.3985424

Dataset 06: DOI 10.5281/zenodo.3986526

Dataset 07: DOI 10.5281/zenodo.3986580

Acknowledgements

We would like to thank Silvie Muschter and Annette Teichman for conducting the cell culture and Gudrun Holland, Petra Kaiser, Freya Kaulbars and Lars Möller for embedding of the samples. We are also grateful to Christoph Schaudinn for reading of the manuscript and his valuable suggestions and to Ursula Erikli for copy-editing.

Author contributions

M.L. designed the study and wrote the manuscript; A.K., T.H., M.L. performed the EM investigations; J.M. and A.N. planned the cell culture and infection experiments, including their quality assurance. All authors discussed the results and their presentation and approved the final version.

Additional information

Supplementary information accompanies this paper.

All image data used for the measurements are available at the Zenodo research data repository.

Competing interests

The authors declare no competing interests.

Figure Legends

Figure 1. Transmission EM of a single virus particle of SARS-CoV-2 at the surface of a Vero cell in an ultrathin plastic section (10 summed up digital slices of an electron tomogram). The section through the virus particle shows the main ultrastructural features of the virus which were manually highlighted by color: yellow = virus-enveloping membrane, red = peplomer (spike protein), blue = ribonucleoprotein (N protein and RNA). Scale bar = 100 nm.

Figure 2. Transmission EM of ultrathin sections through Vero cells which were either infected with SARS-CoV (**A**), or with SARS-CoV-2 (**B**). Viruses are attached to the surface of the cells and do not reveal substantial differences in their ultrastructure. Scale bars = 100 nm.

Figure 3. Particle size distribution of SARS-CoV and SARS-CoV-2. **A, B.** Histograms of maximal particle profile diameter in ultrathin (60-70 nm) sections (datasets 01 and 02; Table 1). **C, D.** Histograms of maximal particle profile diameter without peplomers in ultrathin (60-70 nm) sections (datasets 01 and 02; Table 1). **E, F.** Histograms of maximal particle profile diameter without peplomers in electron tomograms of thin (150-180 nm) sections (datasets 04 and 05; Table 1). Particles were measured at their thickest diameter (see Fig. 4 and Methods section). M = median; N = number of measured particles.

Figure 4. A single digital slice (z view) of an electron tomogram of SARS-CoV-2 particles. The ortho-slice view shows the particle labelled by the white cross lines in side view (x/z and y/z) of the volume at the indicated section plane. The particle appears ovoid in shape and the thickest part of the particle in z was selected for size measurement. Note that the section is compressed in z and thinner than the nominal 180 nm set at the microtome, which also affects the shape of the particle viewed in x/z and y/z. This artifact is well known in electron tomography of plastic sections and only slightly affects the size in x/y[16]. Scale bar = 100 nm.

Figure 5. Analysis of the peplomer density of SARS-CoV and SARS-CoV-2 by transmission EM of very thin (45 nm) ultrathin sections. **A, B.** Single virus particles of either SARS-CoV (**A**) or SARS-CoV-2 (**B**) which show differences in peplomer density. Scale bars = 100 nm. **C, D.** Histograms of the number of peplomers per unit perimeter membrane length of SARS-CoV (**C**) and SARS-CoV-2 (**D**) (datasets 06 and 07; Table 1). M = median; N = number of measured particles.

References

1. Tang, D., Comish, P. & Kang, R. The hallmarks of COVID-19 disease. *PLoS Pathog.* **16**, e1008536; 10.1371/journal. ppat.1008536 (2020).

2. Martines, R. B. *et al.* Pathology and pathogenesis of SARS-CoV-2 associated with fatal coronavirus disease, United States. *Emerg. Infect. Dis.* **26**, 2005-2015; 10.3201/ eid2609.202095 (2020).

3. Puelles, V. G. *et al.* Multiorgan and renal tropism of SARS-CoV-2. *New Engl. J. Med.* **383**, 590-592 (2020).

4. Lu, R. *et al.* Genomic characterisation and epidemiology of 2019 novel coronavirus: implications for virus origins and receptor binding. *Lancet* **395**, 565-574 (2020).

5. Hoffmann, M. *et al.* SARS-CoV-2 cell entry depends on ACE2 and TMPRSS2 and is blocked by a clinically proven protease inhibitor. *Cell* **181**, 271-280 (2020).

6. Chu, H. *et al.* Comparative tropism, replication kinetics, and cell damage profiling of SARS-CoV-2 and SARS-CoV with implications for clinical manifestations, transmissibility, and laboratory studies of COVID-19: an observational study. *Lancet Microbe* **1**, e14-23 (2020).

7. Hui, K. P. Y. *et al.* Tropism, replication competence, and innate immune responses of the coronavirus SARS-CoV-2 in human respiratory tract and conjunctiva: an analysis in ex-vivo and in-vitro cultures. *Lancet Resp. Med.* **8**, 687-695 (2020).

8. Lamers, M. M. *et al.* SARS-CoV-2 productively infects human gut enterocytes. *Science* **369**, 50-54 (2020).

9. Ogando, N. S. *et al.* SARS-coronavirus-2 replication in Vero E6 cells: replication kinetics, rapid adaptation and cytopathology. *J. Gen. Virol.*; 10.1099/jgv.0.001453 (2020).

10. Wrapp, D. et al. Cryo-EM structure of the 2019-nCoV spike in the prefusion conformation. *Science* **367**, 1260–1263 (2020).

11. Ke, Z. *et al.* Structures, conformations and distributions of SARS-CoV-2 spike protein trimers on intact virions. *bioRxiv*; 10.1101/2020.06.27.174979v1 (2020).

12. Turoňová, B. *et al.* In situ structural analysis of SARS-CoV-2 spike reveals flexibility mediated by three hinges. *Science*; 10.1126/science.abd5223 (2020).

13. Yao, H. *et al.* Molecular architecture of the SARS-CoV-2 virus. *bioRxiv*; 0.1101/2020.07.08.192104 (2020).

14. Klein, S. *et al.* SARS-CoV-2 structure and replication characterized by in situ cryo-electron tomography. *bioRxiv*; 10.1101/2020.06.23.167064 (2020).

15. Goldsmith, C. S., Miller, S. E., Martines, R. B., Bullock, H. A. & Zaki, S. R. Electron microscopy of SARS-CoV-2: a challenging task. *Lancet* **395**, e99; 10.1016/ S01406736(20)311880 (2020).

16. Thiel, V. *et al.* Mechanisms and enzymes involved in SARS coronavirus genome expression. *J. Gen. Virol.* **84**, 2305–2315 (2003).

17. Colavita, F. *et al*. SARS-CoV-2 isolation from ocular secretions of a patient with COVID-19 in Italy with prolonged viral RNA detection. *Ann. Intern. Med.* **173**, 242-243 (2020).

18. Luft, J. H. Improvements in epoxy resin embedding methods. *J. Biophys. Biochem. Cytol.* **9**, 409-414 (1961).

19. Laue, M. Electron microscopy of viruses. *Method. Cell Biol.* **96**, 1-20 (2010).

20. Schindelin, J. *et al.* Fiji: an open-source platform for biological-image analysis. *Nat. Methods* **9**, 676-682 (2012).

21. Luther, P. K. Sample shrinkage and radiation damage of plastic sections in *Electron Tomography* (ed. Frank, J.) 17-48 (Springer, 2006).

22. Griffiths, G. Fine-structure immunocytochemistry (Springer, 1993).

23. Luft, J. H. Embedding media - old and new in *Advanced Techniques in Biological Electron Microscopy* (ed. Koehler, J. K.) 1-34 (Springer, 1973).

24. Studer, D., Humbel, B. M. & Chiquet, M. Electron microscopy of high pressure frozen samples: bridging the gap between cellular ultrastructure and atomic resolution. *Histochem. Cell Biol.* **130**, 877–889 (2008).

25. Grünewald, K. & Cyrklaff, M. Structure of complex viruses and virus-infected cells by electron cryo tomography. *Curr. Opin. Microbiol.* **9**, 437-442 (2006).

26. Jiang, W. & Tang, L. Atomic cryo-EM structures of viruses. *Curr. Opin. Struc. Biol.* **46**, 122-129 (2017).

27. Lawrence, J. E. & Steward, G. F. Purification of viruses by centrifugation in *Manual of Aquatic Viral Ecology, Chapter 17* (eds. Wilhelm, S. W., Weinbauer, M. G., & Suttle, C. A.) 166–181 (ASLO, 2010).

28. Dent, S. & Neuman, B. W. Purification of coronavirus virions for cryo-EM and proteomic analysis in *Coronaviruses: Methods and Protocols* (Methods in Molecular Biology, vol. 1282; eds. Maier, H.J. *et al.*) 99-108 (Springer, 2015).

29. Danev, R., Yanagisawa, H. & Kikkawa, M. Cryo-electron microscopy methodology: Current aspects and future directions. *Trends Biochem. Sci.* **44**, 837-848 (2019).

30. Miller, S. E. Detection and identification of viruses by electron microscopy. *J. Electron Microsc. Tech.* **4**, 265-301 (1986).

31. Beniac, D., Andonov, A., Grudeski, E. & Booth, T. F. Architecture of the SARS coronavirus perfusion spike. *Nature Struct. Mol. Biol.* **13**, 751-752 (2006).

32. Wagner, R. C. The effect of tannic acid on electron images of capillary endothelial cell membranes. *J. Ultrastruct. Res.* **57**, 132-139 (1976).

33. Hopwood, D. Cell and tissue fixation, 1972–1982. *Histochem. J.* **17**, 389-442 (1985).

34. Korber, B. *et al.* Tracking changes in SARS-CoV-2 spike: evidence that D614G increases infectivity of the COVID-19 virus. *Cell* **182**, 1–16 (2020).

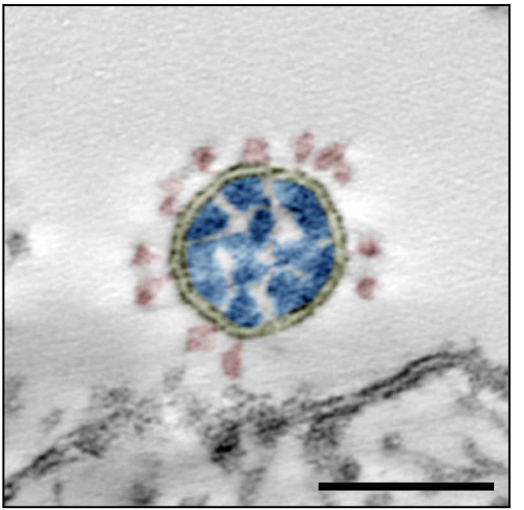

Figure 1

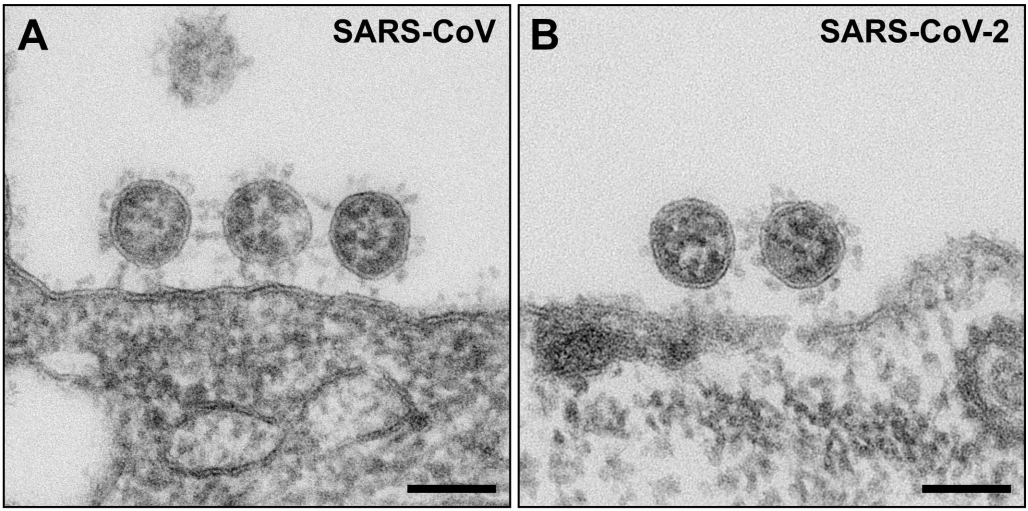

Figure 2

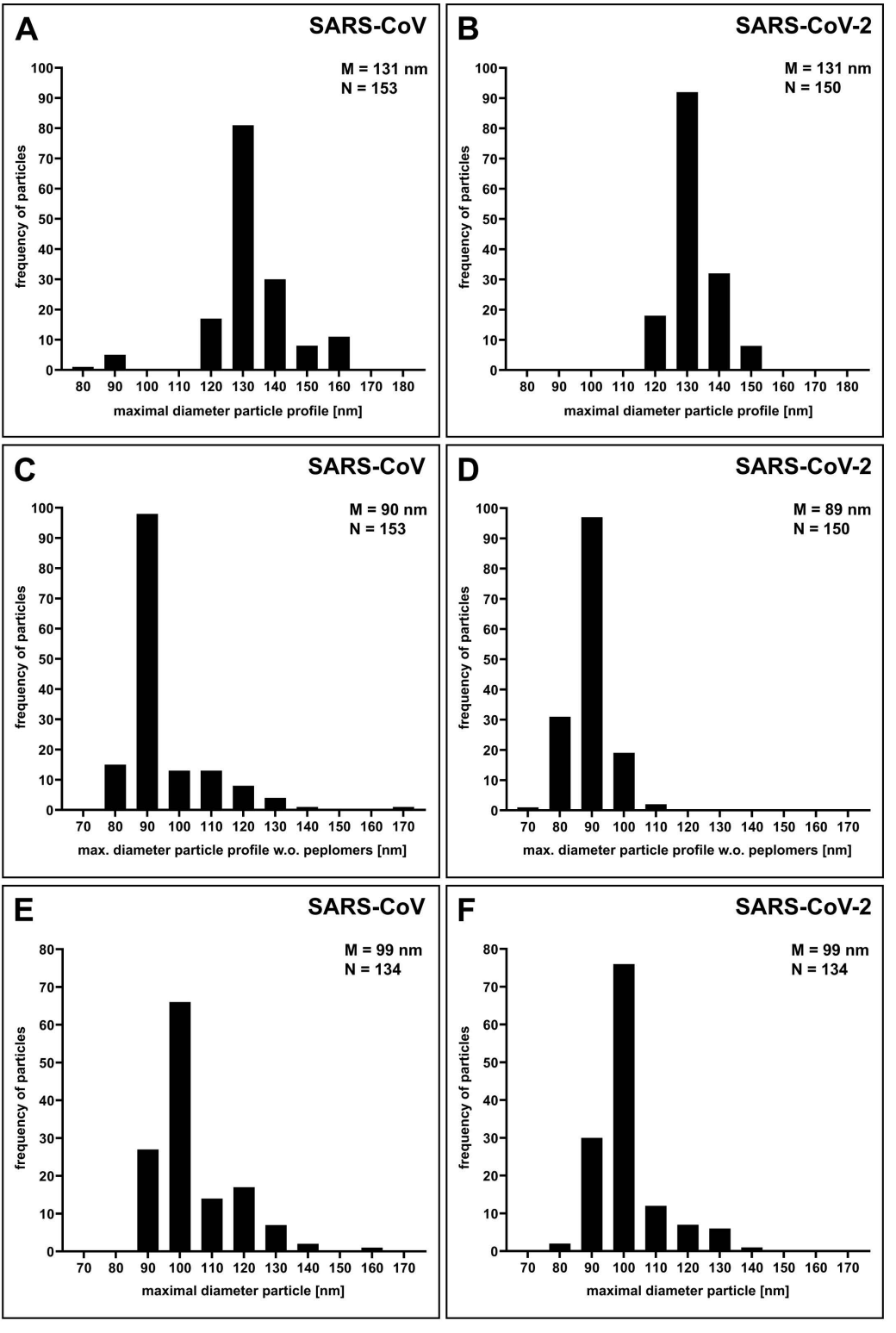
A
SARS-CoV
M = 131 nm
N = 153
frequency of particles
maximal diameter particle profile [nm]
B
SARS-CoV-2
M = 131 nm
N = 150
frequency of particles
maximal diameter particle profile [nm]
C
SARS-CoV
M = 90 nm
N = 153
frequency of particles
max. diameter particle profile w.o. peplomers [nm]
D
SARS-CoV-2
M = 89 nm
N = 150
frequency of particles
max. diameter particle profile w.o. peplomers [nm]
E
SARS-CoV
M = 99 nm
N = 134
frequency of particles
maximal diameter particle [nm]
F
SARS-CoV-2
M = 99 nm
N = 134
frequency of particles
maximal diameter particle [nm]

Figure 3

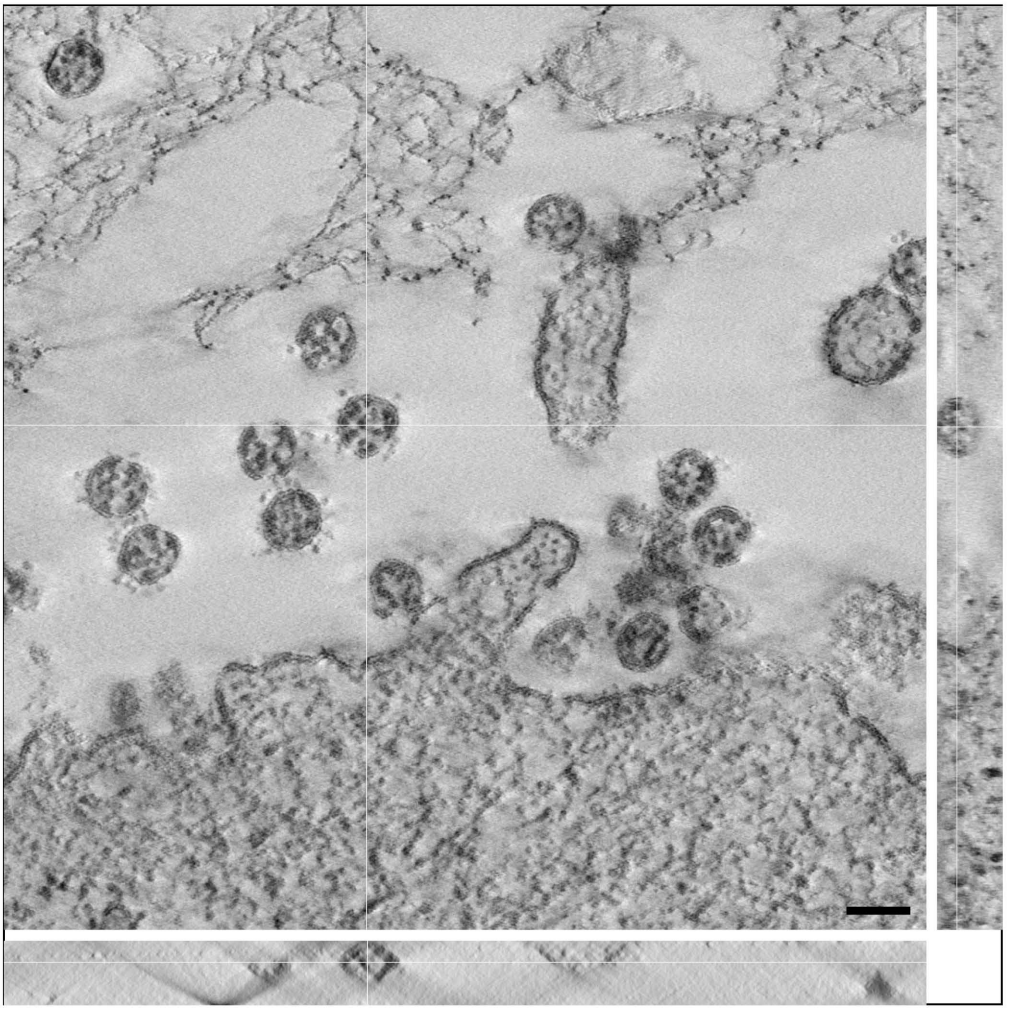

Figure 4

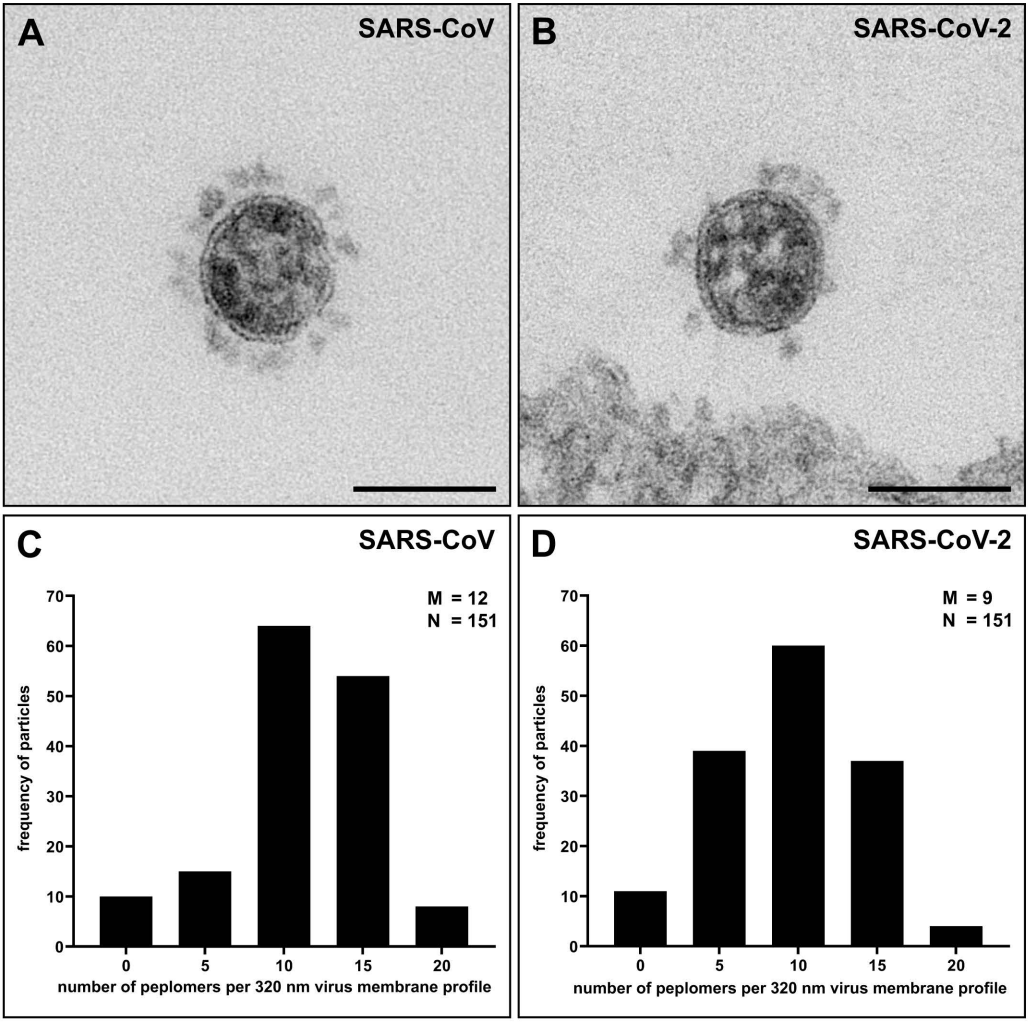
A
SARS-CoV
B
SARS-CoV-2
C
SARS-CoV
M = 12
N = 151
frequency of particles
0
10
20
30
40
50
60
70
0
5
10
15
20
number of peplomers per 320 nm virus membrane profile
D
SARS-CoV-2
M = 9
N = 151
frequency of particles
0
10
20
30
40
50
60
70
0
5
10
15
20
number of peplomers per 320 nm virus membrane profile

Figure 5